Journal of Biomedical Optics

SPIEDigitalLibrary.org/jbo

Targeted zwitterionic near infrared fluorescent probe for improved imaging of type 2 cannabinoid receptors

Zhiyuan Wu
Pin Shao
Shaojuan Zhang
Mingfeng Bai

SPIE

Targeted zwitterionic near infrared fluorescent probe for improved imaging of type 2 cannabinoid receptors

Zhiyuan Wu,[a,b,†] Pin Shao,[a,†] Shaojuan Zhang,[a,c] and Mingfeng Bai[a,d,*]
[a]University of Pittsburgh, Department of Radiology, Molecular Imaging Laboratory, Pittsburgh, Pennsylvania 15219
[b]Shanghai Jiao Tong University, School of Medicine, Ruijin Hospital, Department of Radiology, Shanghai 200025, China
[c]Xi'an Jiaotong University, the First Hospital of Medical School, Department of Diagnostic Radiology, Xi'an, Shaanxi 710061, China
[d]University of Pittsburgh Cancer Institute, Pittsburgh, Pennsylvania 15232

Abstract. Recent studies indicate that the type 2 cannabinoid receptors (CB_2R) have become an attractive target for treating a variety of pathologies, including cancers, neurodegenerative diseases, inflammation, pain, osteoporosis, immunological disorders and drug abuse. In addition, it appears that many of these diseases have up-regulated CB_2R expression. However, the precise role of CB_2R in the regulation of diseases remains unclear. The ability to specifically image CB_2R would contribute to develop reliable CB_2R-based therapeutic approaches with a better understanding of the mechanism of CB_2R action in these diseases. We developed a CB_2R-targeted zwitterionic near-infrared (NIR) fluorescent probe, ZW760-mbc94. When compared with a previously reported CB_2R probe (NIR760-mbc94) with the same targeting moiety but a charged NIR fluorescent dye, ZW760-mbc94 showed improved binding specificity *in vitro* and *ex vivo*. Overall, ZW760-mbc94 appears to have great potential as a CB_2R-targeted contrast agent. [DOI: 10.1117/1.JBO.19.3.036006]

Keywords: near infrared; fluorescent; probe; type 2 cannabinoid receptor; zwitterionic; optical imaging.

Paper 130915R received Dec. 30, 2013; revised manuscript received Jan. 27, 2014; accepted for publication Jan. 30, 2014; published online Mar. 6, 2014.

1 Introduction

The type 2 cannabinoid receptors (CB_2R) are G protein-coupled receptors (GPCR) that belong to the endocannabinoid signaling system. They play a fundamental role in the regulation of a variety of physiopathological processes involving the immune system, including diseases that affect the cardiovascular and respiratory systems, bone remodeling and gastrointestinal, and liver diseases.[1] Under healthy conditions, high-CB_2R expression is present only in B cells of the immune system that are localized in spleen and lymph nodes.[2] In a number of additional cell types under disease conditions, CB_2R expression is greatly up-regulated.[3] The richness of CB_2R involvement has positioned the receptor as an attractive therapeutic target for treating an array of pathologies, such as cancers,[4,5] neurodegenerative diseases,[2,6] inflammation,[7,8] pain,[9] osteoporosis,[10] immunological disorders,[11–13] and drug abuse.[14] As such, there has been an explosion of research over the past 12 years that focused on the biology and therapeutic promises of CB_2R. However, the precise role of CB_2R in the regulation of diseases remains unclear.[15] The ability to specifically image CB_2R would contribute to develop reliable CB_2R-based therapeutic approaches with a better understanding of the mechanism of CB_2R action in these diseases.

Molecular imaging (MI) has emerged as a valuable tool for the visualization, characterization, and measurement of biological processes at the molecular and cellular levels in humans and other living systems.[16] To overcome the current challenge of identifying CB_2R, we therefore set out to develop MI tools that can specifically label CB_2R, quantify the expression level and image the receptor in a living system. One clear strength of CB_2R-targeted MI agents is the potential for high-contrast imaging. CB_2R expression is high only in spleen and lymph nodes, and low—or even undetectable—in brain, thyroid, retina, placenta, skeletal muscle, kidney, liver, adrenal gland, heart, prostate, and ovary.[17,18] This allows for imaging of physiological CB_2R activity in the immune system with low background elsewhere. In certain pathological conditions, CB_2R expression is greatly up-regulated in the diseased cells. For example, CB_2R is over-expressed in various types of cancers,[19] endometrial inflammation,[20] and atherosclerotic plaques.[21] CB_2R expression also increases in diseased central nervous system cells, including astrocytomas,[22] activated microglia and neurons,[14,15,23] astrocytes of Alzheimer's disease,[24] as well as T-lymphocytes, microglia, and astrocytes in multiple sclerosis.[25] Because CB_2R expression is nearly absent in these areas under basal conditions, and increases as much as 100-fold in diseases,[3] CB_2R imaging can achieve a high-imaging contrast in diseased tissues. Accordingly, CB_2R is a promising target for MI applications.

CB_2R imaging remains a largely unexplored field. Few CB_2R contrast agents that can identify the receptor specifically at the cellular scale have been developed. We recently reported a CB_2R-targeted near-infrared (NIR) fluorescent probe, NIR760-mbc94, which was successfully used to image the receptor *in vitro* and *in vivo*.[26] Although the specific binding of NIR760-mbc94 to CB_2R has been demonstrated, the probe also showed

*Address all correspondence to: Mingfeng Bai, E-mail: baim@upmc.edu

†These authors equally contributed to this work.

0091-3286/2014/$25.00 © 2014 SPIE

nonspecific binding. Specifically, SR144528, a CB_2R ligand, partially inhibited the uptake of NIR760-mbc94 *in vitro* (40%) and *ex vivo* (35%).[26] Recently, Dr. Frangioni's group found that replacing charged NIR fluorescent dyes with a zwitterionic (net charge = 0) NIR dye significantly reduced the nonspecific binding of integrin $\alpha_v\beta_3$-targeted imaging agents.[27] Inspired by this report, in this study, we introduced zwitterionic properties into our CB_2R-targeted agents. We found that our zwitterionic CB_2R probe, ZW760-mbc94, enhanced blocking effect from 40% to 50% *in vitro* and 35% to 47% *ex vivo* when compared with NIR760-mbc94. Such improvement may greatly improve the outcome of CB_2R-targeted imaging.

2 Methods and Materials

2.1 *Synthesis of CB_2R-Targeted Zwitterionic NIR Probe ZW760-mbc94*

The solvents used are of commercial grade. The precursor dye ZW-Cl and the ligand mbc94 were synthesized using the previously reported procedure.[18,28] A Biotage (Charlotte, North Carolina) microwave reactor (model: Initiator$^+$ US/JPN 356007) was employed for the synthesis of the dye ZW760. Flash column chromatography was performed on a Teledyne ISCO (Lincoln, Nebraska) (combiflash RF) purification system with silica gel (standard grade, 60A, Sorbtech, Norcross, Georgia) or C18-reversed phase silica gel (20 to 40 μm, RediSepRf). ^{1}H and ^{13}C nuclear magnetic resonance (NMR) spectra were recorded on a Brucker Avance III 400-MHz instrument. Mass spectra were recorded on a Waters LCT Premier mass spectrometer. UV/Vis spectra were recorded on a Cary 100 Bio UV−Vis spectrophotometer, and fluorescence spectra were recorded on a Cary Eclipse fluorescence spectrophotometer.

ZW760. Dye ZW-Cl (70 mg, 78 μM), 4-Carboxyphenylboronic acid (20 mg, 120 μM) and catalyst tetrakis(triphenylphosphine)palladium(0) were suspended in water (7 mL). The mixture was heated to 160°C and stirred at this temperature for 30 min under the microwave reactor. ZW760 was collected as a green solid (15 mg, 20%) after purification over a C18-reversed phase column using H_2O/MeOH (20% MeOH to 100% MeOH) as the eluent. ^{1}H NMR (*d*4-MeOD): $\delta = 8.21$ (d, 2 H, $J = 7.6$ Hz), 7.97 (d, 2 H, $J = 8$ Hz), 7.74 (d, 2 H, $J = 8.4$ Hz), 7.68 (s, 2 H), 7.16-7.2 (m, 3 H), 7.09 (d, 2 H, $J = 8.4$ Hz), 6.24 (d, 2 H, $J = 14$ Hz), 3.98 (br.s, 4 H), 3.51 to 3.55 (m, 4 H), 3.16 (s, 18 H), 2.79 (t, 4 H, $J = 5.6$ Hz), 2.18 (br.s, 4 H), 2.06 to 2.09 (m, 2 H), 1.07 (s, 12 H). MS (ESI): $m/z = 899.24$, calcd. for $C_{49}H_{63}N_4O_8S_2$ $[M]^+$ $m/z = 899.41$.

ZW760-mbc94. A mixture of ZW760 (11 mg, 11 μmol), HBTU (5 mg, 13 μmol), and HOBt (1.8 mg, 13 μmol) in anhydrous DMF (2.5 mL) was stirred at room temperature for 10 min. DIEA (3 μL, 17 μmol) was then added and the resulting mixture was stirred for another 10 min. After a solution of mbc94 (7 mg, 12 μmol) in anhydrous DMF (1 mL) was added, the reaction mixture was stirred at room temperature under argon atmosphere in the absence of light for 24 h. The solvent was then removed by rotary evaporation and the resulting solid was purified by semipreparative high-performance liquid chromatography using a Phenomenex (Torrance, California) Luna C-18 column (250 × 10 mm) at a flow rate of 4 mL/min. Flow A was 0.1% trifluoroacetic acid (TFA) in water and flow B was 0.1% TFA in acetonitrile. The elution method started with a linear gradient from 40% to 100% B over 30 min, held at 100% B for 5 min, and finally returned to 40% B over 5 min. After being dried by lyophilization, ZW760-mbc94 (3.4 mg, 20%) was obtained as a green solid. ^{1}H NMR (*d*4-MeOD): $\delta = 8.71$ (t, 1H, $J = 6$ Hz), 8.15 (d, 2 H, $J = 8.8$ Hz), 7.82(dd, 2 H, $J = 8$ & 1.6 Hz), 7.7 (s, 2 H), 7.5 (d, 2 H, $J = 8$ Hz), 7.4 (*d*, 1 H, $J = 8.4$ Hz), 7.32 to 7.37 (m, 6 H), 7.27 (d, 2 H, $J = 14$ Hz), 7.2 (dd, 1 H, $J = 7.6$ & 1.6 Hz), 7.12 (d, 2 H, $J = 8$ Hz), 6.85 (s, 1 H), 6.32 (d, 2 H, $J = 14$ Hz), 5.51 (s, 2 H), 4.2 (m, 5 H), 3.77 (*d*, 1 H, $J = 7.6$), 3.48 to 3.58 (m, 6 H), 3.17 (s, 18 H), 3.07 (t, 2 H, $J = 8$ Hz), 2.8 (t, 4 H, $J = 6$ Hz), 2.36 (s, 3 H), 2.26 to 2.28 (m, 4 H), 2.06 to 2.07 (m, 2 H), 1.73 to 1.80 (m, 7 H), 1.49 to 1.53 (m, 6 H), 1.19 (s, 12 H), 1.16 (s, 3H), 1.09 (s, 3 H), 0.87 (s, 3 H). ^{13}C NMR (*d*4-MeOD): $\delta = 174.01$, 168.65, 164.14, 150.58, 144.58, 143.44, 142.02, 139.76, 138.04, 136.51, 135.78, 135.72, 134.18, 132.57, 132.24, 131.67, 131.64, 130.92, 130.58, 128.95, 128.88, 128.61, 128.19, 121.32, 111.30, 108.21, 101.97, 64.91, 64.52, 53.77, 43.69, 40.71, 31.48, 30.49, 28.12, 28.02, 27.83, 27.54, 26.90, 25.55, 22.17, 21.67, 20.04. MS (ESI): $m/z = 490.57$, calcd. for $C_{84}H_{111}ClN_9O_8S_2$ $[M+2H]^{3+}$ $m/z = 490.92$.

2.2 *Cell Culture and Animal Model*

A mouse malignant astrocytoma cell line transfected with CB_2R, CB_2-mid delayed brain tumor (DBT), which expresses CB_2R at endogenous level, was used to test the efficiency of the probe *in vitro* and *in vivo*.[29] Cells were cultured in Dulbecco's-modified Eagle's medium supplemented with 10% heat-inactivated fetal bovine serum, 4-mM glutamine, 100-units/ml penicillin and 100-μg/ml streptomycin.

Subcutaneous tumors of CB_2-mid DBT were induced subcutaneously into the flank of 6- to 8-week-old female Nu/nu mice by injecting 1×10^6 subconfluent cells in 100-μL phosphate buffered saline (PBS). All studies were performed in accordance with institutional guidelines for animal use after obtaining approval for the experimental protocols from University of Pittsburgh.

2.3 *In Vitro Saturation Binding Assay*

Intact cell saturation binding assay was carried out to determine the binding affinity of ZW760-mbc94 to CB_2R using a similar method as we previously reported.[26] Briefly, CB_2-mid DBT cells were seeded onto 96 well optical bottom plates with 5000 cells per well and incubated for 24 h. Hank's balanced salt solution with 1 mM Mg^{2+}, 0.1% BSA, 0.1% NaN_3 was used as the binding buffer. Cells were incubated for 30 min with an increasing concentration of ZW760-mbc94 (2.0, 5.0, 10.0, 40.0, 100.0, and 160.0 nM) at 37°C. For nonspecific binding measurements, 1 μM (final concentration) of the blocking agent 4-Quinolone-3-Carboxamide (4Q3C, Cayman Chemicals) was added with ZW760-mbc94 to each well, while for total binding measurements, no blocking agent was added. Cells were then rinsed with serum free medium and fluorescence intensity at 790 nm (relative fluorescence units) was recorded with a Synergy H4 hybrid multimode microplate reader. DRAQ-5, a commonly used cell nuclear DNA labeling dye, was used to normalize cell numbers based on fluorescence intensity at 690 nm (excited at 650 nm) using the protocol provided by the manufacturer. The specific binding was obtained by the subtraction of nonspecific binding from total binding. The dissociation constant (K_d) and

receptor density (Bmax) were estimated from the nonlinear fitting of specific binding versus of ZW760-mbc94 concentration using Prism software (GraphPad Prism 6.01, San Diego, California).

2.4 *In Vitro Fluorescence Imaging of ZW760-mbc94*

Fluorescence microscopy was performed using a Zeiss Axio Observer (Carl Zeiss MicroImaging, LLC, Thornwood, New York) fluorescence microscope equipped with the ApoTome 2 imaging system. ZW760-mbc94 or ZW-acid (free dye control) fluorescence images were captured using a NIR camera with an indocyanine green (ICG) filter set (excitation/emission: 750 to 800 nm/820 to 875 nm). Nuclear images were obtained with a 4',6-diamidino-2-phenylindole (DAPI) filter set (excitation/emission: 335 to 383 nm/420 to 470 nm). Differential interference contrast (DIC) images were obtained through Trans light DIC. A multiplate reader system (Synergy H4) was used for quantitative analysis of the fluorescent probe uptake (excitation /emission = 740/790 nm).

Cells were divided to four groups to test the binding specificity of ZW760-mbc94 to CB_2R: (1) CB_2-mid DBT cells treated with 5 μM of ZW760-mbc94 for 30 min; (2) CB_2-mid DBT cells treated with 5 μM of ZW760-mbc94 together with 10 μM of 4Q3C as the blocking agent for 30 min; (3) CB_2-mid DBT cells treated with 5 μM of free ZW760 dye without targeting moiety for 30 min; and (4) wild type (WT) DBT-cells (CB_2R-)-treated with 5 μM of ZW760-mbc94 for 30 min. All experiments were carried out at 37°C. CB_2-mid DBT cells and WT DBT-cells were plated at 5000 cells per well in 8-well chamber slides (for fluorescence microscopy) or 96-well plates (for quantitative optical imaging using multiplate reader) 24 h before the treatment. ZW760-mbc94 with or without 4Q3C, or free ZW760 was added to cells in culture medium. After being incubated for 30 min, the cells were washed three times with serum-free medium and fixed with 4% paraformaldehyde/PBS for 20 min at room temperature. The cell nucleus was stained with 1-μg/mL DAPI for 15 min at room temperature. Each group of cells was triplicated.

2.5 *In Vivo Optical Imaging*

Animal experiments were conducted in accordance with the guidelines for the Care and Use of Laboratory Animals of the Medical Research Council of University of Pittsburgh. NIR-based fluorescent imaging was performed with a Xenogen IVIS Spectrum imaging system (IVIS Lumina XR; excitation, 745 nm; emission, 800 nm; exposure time, 1 s; binning, small; field of view, 10; f/stop, 2; open filter). Imaging and quantification of signals were controlled by the acquisition and analysis software Living Image 2.5 software (Xenogen, Alameda, California). Experiments with tumor-bearing mice were performed 10 days after the injection of tumor cells when the tumor size reached 6 to 7 mm in diameter. Mice were divided into three groups, each of which was injected with the following agents (dissolved in 100-μL saline) via the tail vein: three mice with 10-nmol ZW760-mbc94, three with 10-nmol ZW760-mbc94 + 100 nmol 4Q3C, and three with 10-nmol free ZW760 dye. Mice were anesthetized by continuous exposure to 2.5% isoflurane. Images at the following time points were collected: preinjection, 0.02-, 0.5-, 1-, 2-, 4-, 6-, 12-, 24-, 48-, and 72-h postinjection (PI). The signal intensity was expressed as the average radiance $[(\text{photons/s/cm}^2\text{/sr})/(\mu\text{W/cm}^2)]$. To determine tumor contrast, the radiant efficiency of the tumor area at the right flank of the animal (T) and of the area at the left leg muscle [normal tissue (N)] was calculated by the region of interest (ROI) function of Living Image software. The ratio of T/N is the contrast between the tumor and normal tissue.

2.6 *Ex Vivo Optical Imaging and Biodistribution*

After the last imaging time point (72-h PI), tumor-bearing mice were sacrificed by cervical dislocation under isoflurane anesthesia. The tumor and organs (blood, heart, lung, liver, spleen, pancreas, kidney, muscle, and brain) were collected for *ex vivo* optical imaging studies and biodistribution analysis. The *ex vivo* imaging contrast was calculated by comparing the average fluorescence intensities in the tumor with that in the left leg muscle from the same animal.

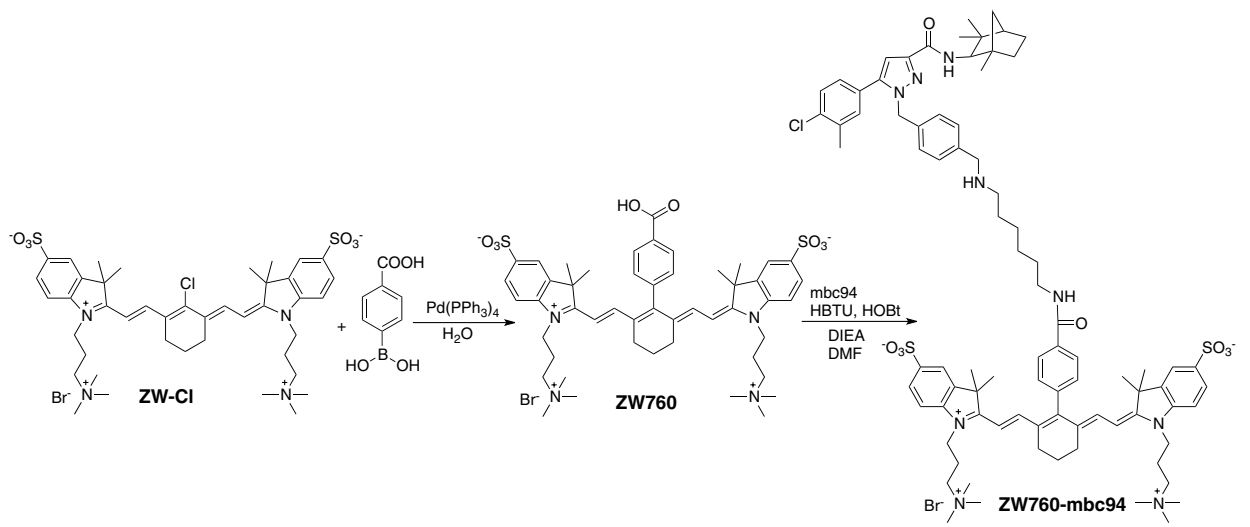

Fig. 1 Synthetic pathway of ZW760-mbc94.

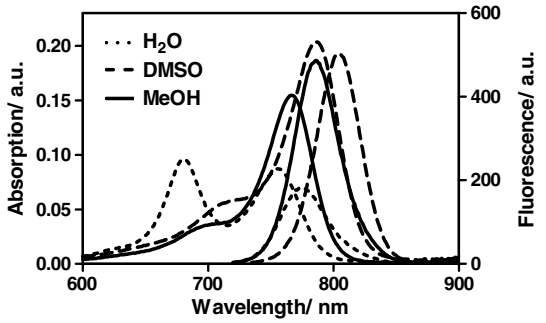

Fig. 2 UV–Vis absorption and emission of ZW760 and ZW760-mbc94 in water at a concentration of 1 μM ($\lambda_{ex} = 700$ nm).

2.7 *Statistical Analysis*

All of the data were given as the mean ± standard deviation of n independent measurements. The results were evaluated using the IBM statistical software (SPSS Statistics version 21). Student's t-test (two tailed) was applied for the analysis of statistical differences. P value < 0.05 was considered to be statistically significant.

3 Results and Discussion

The structure of the CB_2R-targeted zwitterionic probe, ZW760-mbc94, was designed with the following considerations: (1) We chose mbc94 as the targeting moiety, which was previously reported by us to have specific binding to CB_2R.[3,18,26] (2) We developed a novel zwitterionic NIR dye, ZW760, which has a robust C—C linkage at the meso position of the polymethine chain, as compared with the enol ether linkage in the recently reported ZW800 dyes.[28] Previous studies indicate that heptamethine cyanine dyes with an enol ether linkage have significant stability issues, which can be overcome by replacing the enol ether with a C—C linkage.[26,30] In addition, the carboxylate group on ZW760 allows for universal conjugation to various targeting moieties.

ZW760-mbc94 was synthesized by following the pathway described in Fig. 1. Briefly, we first prepared ZW-Cl and mbc94 using the previously reported methods.[18,28] Next,

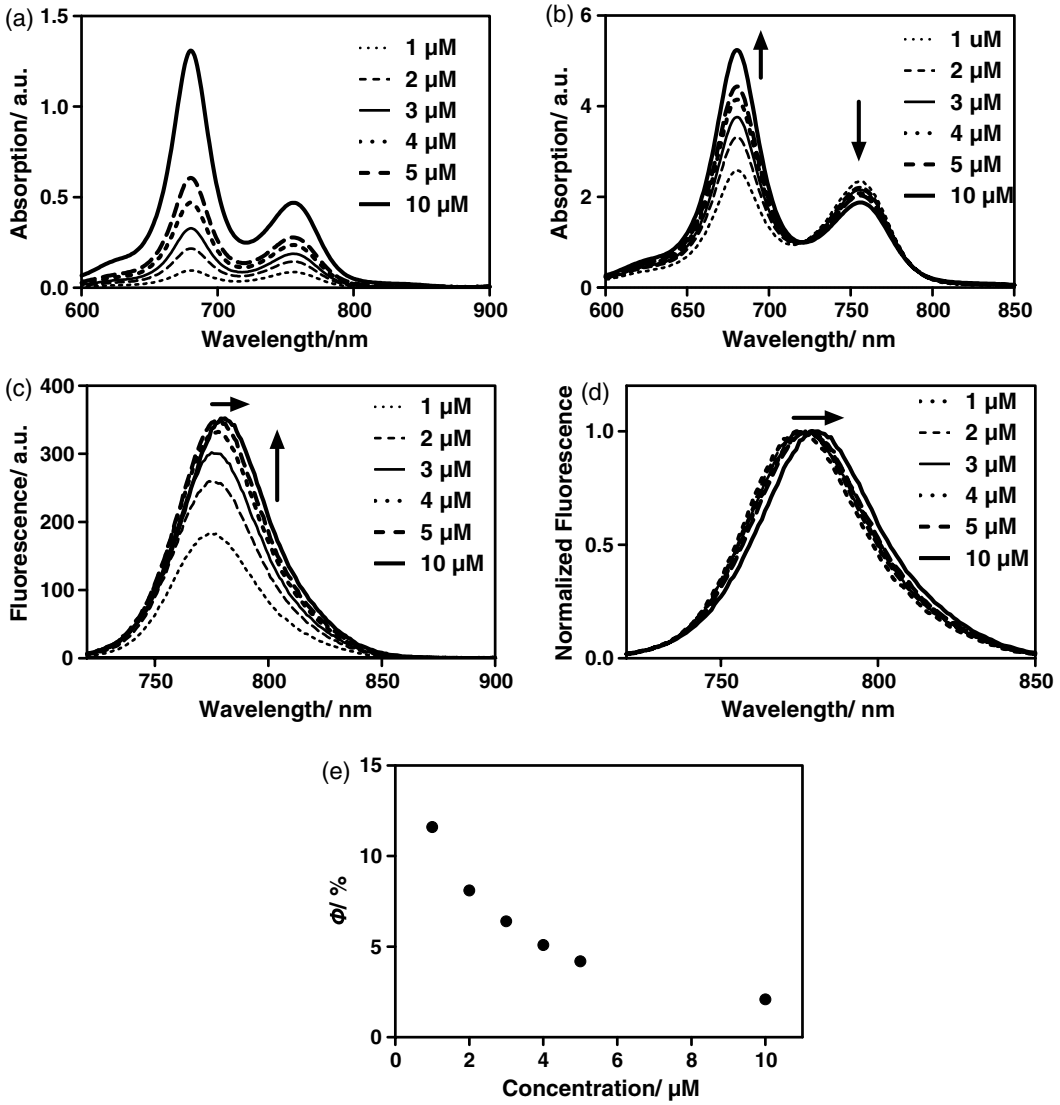

Fig. 3 The concentration-dependent spectra of ZW760 in water. (a) UV–Vis absorption spectra; (b) absorption spectra normalized at 720 nm; (c) emission spectra; (d) the normalized emission spectra ($\lambda_{ex} = 700$ nm); and (e) the concentration-dependent fluorescence quantum yield change.

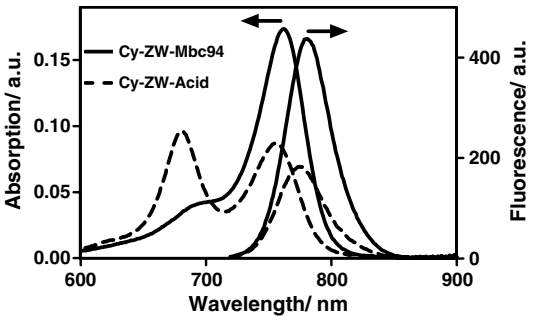

Fig. 4 UV–Vis absorption (solid) and emission spectra (dash) of ZW760 (red) and ZW760-mbc94 (black) in water at a concentration of 1 μM ($\lambda_{ex} = 700$ nm).

Suzuki-Miyaura coupling reaction between 4-carboxyphenylboronic acid and ZW-Cl in the presence of $Pd(PPh_3)_4$ yielded ZW760. Finally, mbc94 was coupled to ZW760 using an amide-coupling reaction.

Upon the syntheses of ZW760 and ZW760-mbc94, we characterized the spectroscopic properties of these two-fluorescent molecules. When dissolved in methanol or dimethyl sulfoxide (DMSO), ZW760 molecules exist mainly as monomers at a concentration of 1 μM, as indicated by the absorption spectra (Fig. 2). ZW760 showed an intense absorption peak at 786 nm with a weak shoulder at 720 nm in DMSO. The small-shoulder peak is ascribed to the well-known H-type aggregation.[31] The shape of the ZW760 absorption spectrum in methanol is similar to that in DMSO, except that the absorption peak is blue shifted for 20 nm. ZW760 exhibited strong NIR

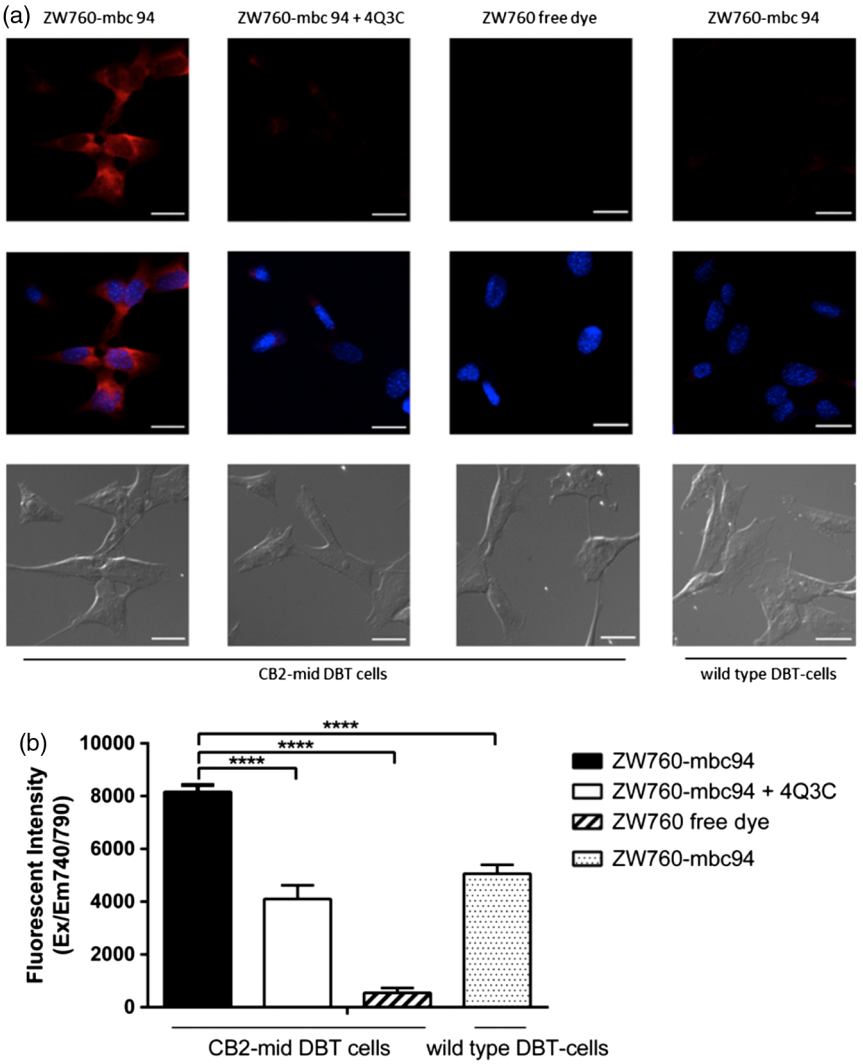

Fig. 5 ZW760-mbc94 specifically binds to CB_2R in CB_2-mid DBT cells. Four groups: (1) CB_2-mid DBT cells treated with 5 μM of ZW760-mbc94 without the blocking agent; (2) CB_2-mid DBT cells treated with 5 μM of ZW760-mbc94 together with 10 μM of 4Q3C; (3) CB_2-mid DBT cells treated with 5 μM of free ZW760 dye; (4) wild type DBT-cells (CB_2R-) treated with 5 μM of ZW760-mbc94. All cells were incubated at 37°C for 30 min and washed three times with serum free medium. (a) Fluorescence images were obtained using a Zeiss Axio Observer fluorescent microscopy with ApoTome 2 imaging system. From top to bottom: ICG filter (red), ICG filter (red) + DAPI filter (blue) merged, differential interference contrast (DIC). Scale: 20 μm. (b) Quantitative fluorescent signal was measured using a Synergy™ H4 hybrid multimode microplate reader. Each data point represents the mean ± standard deviation (SD) based on triplicate samples. (****$p < 0.0001$).

fluorescence in methanol and DMSO. The fluorescent peak is located at 805 and 786 nm in DMSO and methanol, respectively. When water was used as the solvent, ZW760 showed two major absorption bands at 681 and 756 nm with molar extinction coefficient of 9.6×10^4 and 8.7×10^4 M^{-1} cm^{-1}, respectively. As discussed above, the strong absorption at 681 nm is ascribed to the H-aggregation of the dye in water. The aggregation of ZW760 in water was further evidenced by the concentration dependent absorption studies. When the concentration of ZW760 increased from 1×10^{-6} to 1×10^{-5} M in water, the intensity of the two absorption bands increased simultaneously [Fig. 3(a)]. However, the ratio of absorption at 681 nm/756 nm increased greatly [Fig. 3(b)], indicating enhanced H-aggregation at higher concentration. As expected, the fluorescence quantum yields decreased dramatically when concentration increased [Fig. 3(e)]. Due to the reabsorption effect at high concentration,[32] the fluorescent peaks are red shifted gradually from 775 to 781 nm [Figs. 3(c) and 3(d)].

Attachment of the targeting moiety to ZW760 significantly reduced the aggregation. As displayed in Fig. 4, ZW760-mbc94 showed an intense absorption band centered at 762 nm in water and the band profile is similar to that of ZW760 in DMSO and methanol. This indicated that ZW760-mbc94 existed mainly as monomers in water at the concentration of 1 μM. The dissociation of the aggregate significantly improved the absorption and emission of ZW760-mbc94. Compared with the free dye ZW760, the absorption peak of ZW760-mbc94 is slightly red shifted to 762 nm and the molar extinction coefficient almost doubled (9.6×10^4 and 1.74×10^5 M^{-1} cm^{-1} for ZW760 and ZW760-mbc94, respectively). The emission peak of ZW760-mbc94 is also red shifted from 775 to 781 nm as compared with ZW760. Importantly, the fluorescence quantum yield of ZW760-mbc94 in water is 15.2%, which is 31% higher than that of ZW760 (11.6%).

Cellular uptake of ZW760-mbc94 was investigated in CB_2-mid DBT cells that express CB_2R at endogenous levels.[29] All fluorescence images taken are confocal-like images using a Zeiss Axio Observer fluorescence microscope equipped with the ApoTome 2 imaging system. Figure 5(a) shows fluorescence images of CB_2-mid DBT cells and WT DBT-cells (non-CB_2R expressing control) after incubation with 5 μM of ZW760-mbc94, ZW760-mbc94 + 4-Quinolone-3-Carboxamide (4Q3C, blocking agent), or ZW760 (free dye control) for 30 min at 37° C. Strong-fluorescence signal was shown throughout the intracellular cytoplasm of CB_2-mid DBT cells treated with ZW760-mbc94 probes. No accumulation in the nucleus was observed. It is noteworthy that the cell membrane did not appear to be the primary location of the probe uptake, which may seem unexpected as CB_2R belongs to the transmembrane GPCR family. However, recent studies have shown that CB_2R's distribution was predominantly intracellular in many CB_2R-expressing cell lines.[33] When blocked with 4Q3C, ZW760-mbc94 showed a much lower degree of cellular uptake. Furthermore, no significant fluorescence signal was seen from CB_2-mid DBT cells incubated with the free dye (ZW760) control or WT DBT-cells treated with ZW760-mbc94. The combined fluorescence imaging results indicate that ZW760-mbc94 binds to CB_2R specifically and CB_2R expression in CB_2-mid DBT cells is mainly intracellular.

As mentioned in Sec. 1, the main purpose of this study is to evaluate whether replacing the charged NIR760 dye, with zwitterionic ZW760 dye would significantly reduce the nonspecific binding of CB_2R-targeted imaging agents. To quantitatively study the specific uptake of ZW760-mbc94, we screened CB_2-mid DBT and WT DBT-cells using a multiplate reader. As shown in Fig. 5(b), the uptake of ZW760-mbc94 in CB_2-mid DBT was effectively blocked by 4Q3C (8161.7 ± 211.4 versus 4106.3 ± 421.0, $p < 0.0001$). This roughly 50% blocking effect is higher than our previous result using NIR760-mbc94 as the imaging probe,[26] indicating reduced nonspecific binding. In addition, fluorescence signal from CB_2-mid DBT cells treated with free dye is only 6.6% of that with ZW760-mbc94 (8161.7 ± 211.4 versus 542.7 ± 154.7, $p < 0.0001$). Furthermore, the uptake of ZW760-mbc94 in WT DBT cells was ~40% lower than in CB_2-mid DBT cells (5061.3 ± 272.6 versus 8161.7 ± 211.4, $p < 0.0001$). Therefore, the results provided additional evidence for the specificity of ZW760-mbc94, which was improved over the previously reported NIR760-mbc94 probe.

The specific binding of ZW760-mbc94 to CB_2R was further demonstrated by the *in vitro* fluorescence saturation binding study. ZW760-mbc94 served as the fluorescent ligand and 4Q3C was used as the blocking agent to account for nonspecific binding. A representative saturation binding curve is shown in Fig. 6. Similar to NIR760-mbc94, ZW760-mbc94 binds to CB_2R with a nanomolar affinity ($K_d = 53.9 \pm 13.0$ nM).

To study the targeting specificity of ZW760-mbc94 in living systems, *in vivo* optical imaging was performed ~10 days post-inoculation of CB_2-mid DBT tumor cells subcutaneously. The tumor sizes in all mice showed no significant difference. Three groups of mice (three in each group) were administrated with ZW760-mbc94, ZW760-mbc94 + 4Q3C, and ZW760, respectively. The representative *in vivo* time-dependent fluorescence images are shown in Fig. 7(a). All images are displayed on the same scale to allow for direct visual comparison among the uptake profiles of ZW760-mbc94, ZW760-mbc94 + 4Q3C, and ZW760 dye. The free ZW760 dye showed rather quick clearance profile. Right after the injection, intense fluorescence signal was observed throughout the whole body. Most dye molecules were cleared out only 30 min after injection, and no significant fluorescence signal was observed from the animals after the 1-h PI time point. On the contrary, ZW760-mbc94 showed much slower bioclearance profiles, with or without the blocking

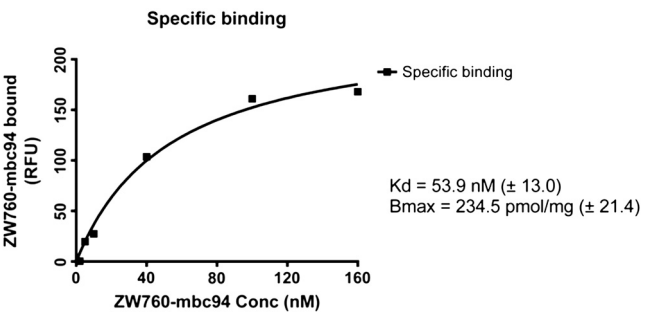

Fig. 6 *In vitro* fluorescence saturation binding assay of ZW760-mbc94. The equilibrium dissociation constant (K_d) and the maximum specific binding (Bmax) were calculated from *in vitro* saturation-binding assay using Prism software. CB_2-mid DBT cells were incubated for 30 min with an increasing concentration of ZW760-mbc94 with or without the blocking agent (4Q3C). Cells were then rinsed with serum free medium and fluorescence at 790 nm was recorded with a Synergy™ H4 hybrid multimode microplate reader. Each data point represents the mean ± SD based on triplicate samples.

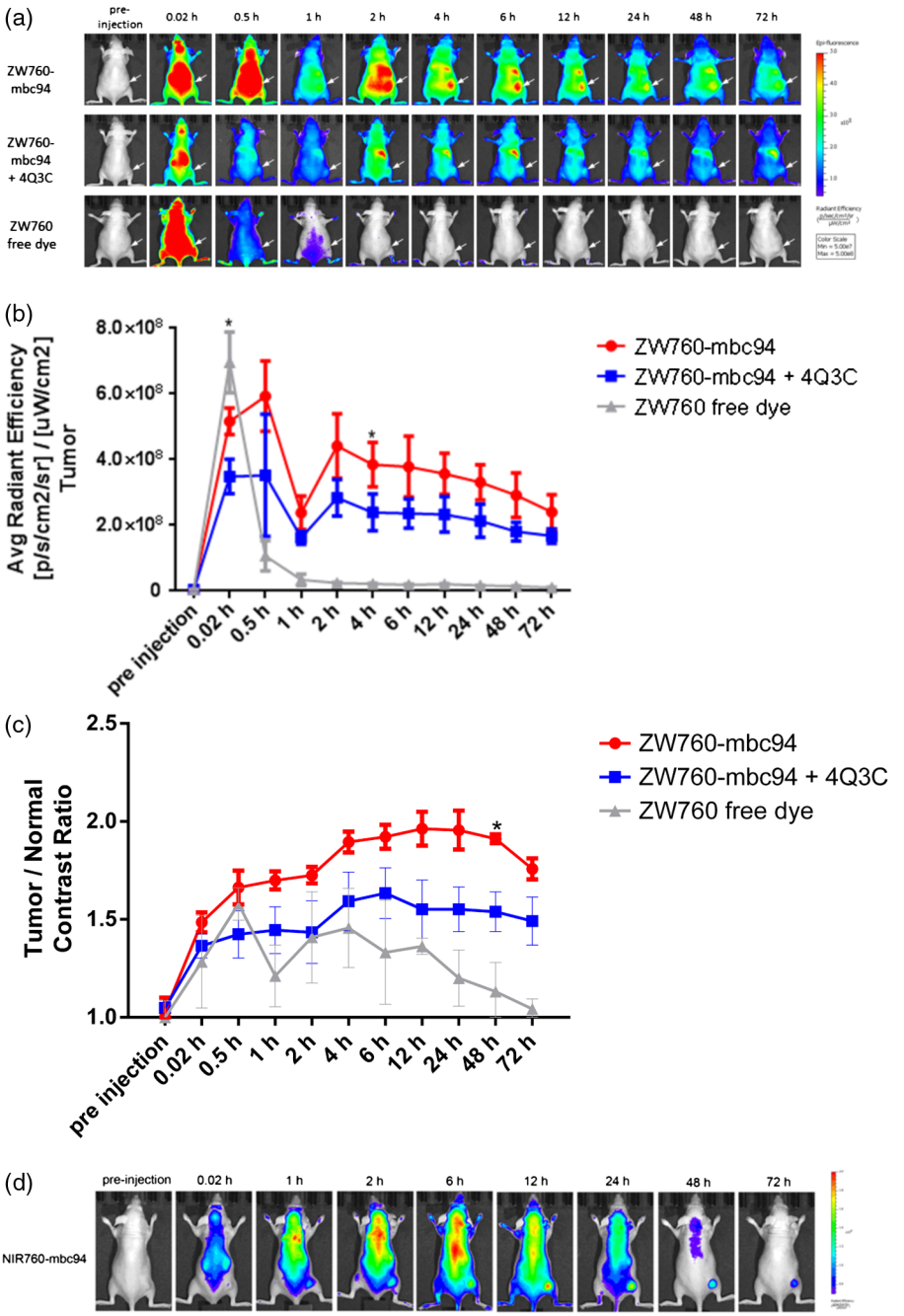

Fig. 7 *In vivo* tumor optical imaging and competitive blocking studies. 1×10^6 CB_2-mid DBT cells were subcutaneously implanted into the right flank of 6- to 8-week-old female Nu/nu mice. Experiments with tumor-bearing mice were performed 10 days after injection of tumor cells. To examine tumor CB_2R-targeted imaging, all mice were injected with the following agents dissolved in 100-μL saline via the tail vein: 3 with 10-nmol ZW760-mbc94, 3 with 10-nmol ZW760-mbc94 + 100 nmol 4Q3C, 3 with 10-nmol free ZW760. (a) Mice were anesthetized with 2.5% isoflurane and imaged with a charge-coupled device camera-based bioluminescence imaging system IVIS Lumina XR, at preinjection, 0.02-, 0.5-, 1-, 2-, 4-, 6-, 12-, 24-, 48-, and 72-h postinjection (PI). (b) Time activity curves of the average radiant efficiency of the tumor area among three groups. Radiant efficiency of the tumor area was calculated by the region of interest (ROI) function of Living Image software. (c) Time activity curves of tumor/background ratio among three groups. Radiant efficiency of the tumor area at the right flank of the animal (T) and of the area at the left flank [normal tissue (N)] was calculated by the ROI function of Living Image software. Dividing T by N yielded the contrast between the tumor tissue and the normal tissue. (d) Previously published *in vivo* imaging results using NIR 760-mbc94 for comparison.[26] *In vivo* images were collected at preinjection, 0.02-, 1-, 2-, 6-, 12-, 24-, 48- and 72-h PI. (*$p < 0.05$).

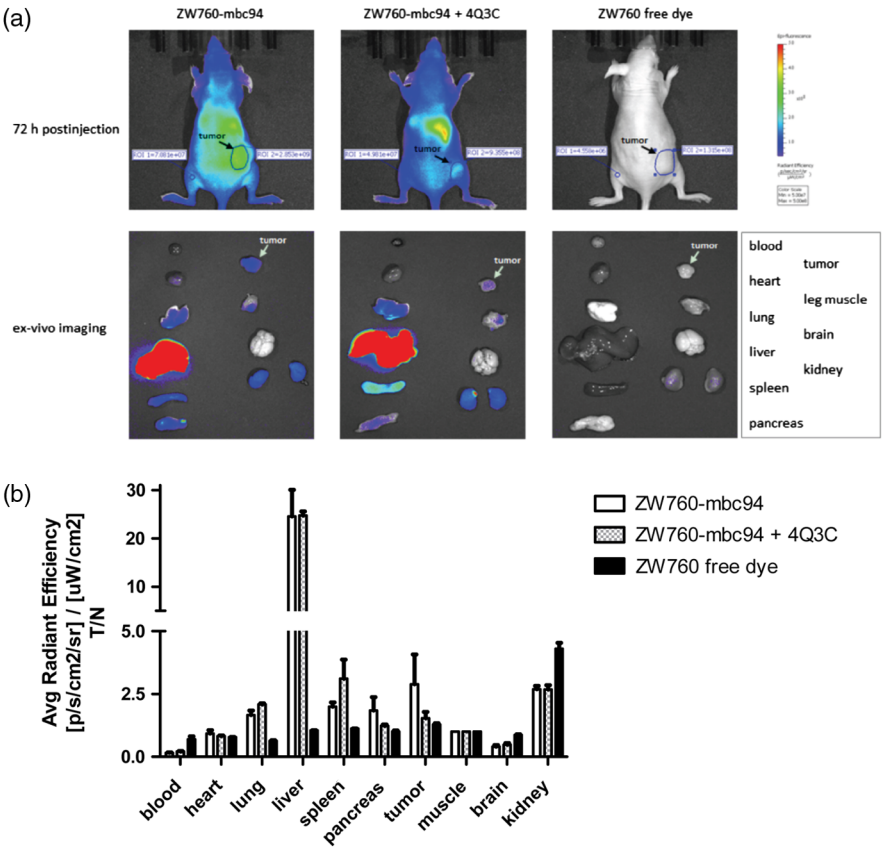

Fig. 8 *Ex vivo* optical imaging and biodistribution study. (a) *Ex vivo* imaging of tumor and selected organs 72-h PI of ZW760-mbc94, ZW760-mbc94 + 4Q3C, or free ZW760 dye. (b) Graphical representation of target/normal contrast ratio for *ex vivo* study, among three groups.

agent (4Q3C). Significant fluorescence signal was observed from the whole body even at the last imaging time point (72-h PI).

The tumor (located at the right flank) of the mice injected with ZW760-mbc94 showed higher fluorescence signal than that in the blocked animals at almost all time points [Fig. 7(b)], with statistical significance ($p < 0.05$) achieved at 4-h PI. The ratio of the fluorescence signal at the tumor area (T) over that at the left leg [normal tissue (N)] was used to calculate the tumor contrast (T/N). For the free dye control mice, intense fluorescent signal was observed throughout the whole body within the first-hour PI without visual tumor contrast, whereas no fluorescence signal was observed anywhere at other time points. For the mice injected with ZW760-mbc94, the T/N ratio gradually increased over time and reached the maximum ($T/N = 1.96 \pm 0.15$) at about 12-h PI [Fig. 7(c)]. Mice treated with ZW760-mbc94 + 4Q3C showed lower T/N ratio at all time points [Fig. 7(c)], with the peak T/N ratio ($T/N = 1.63 \pm 0.22$) at 6-h PI. As shown in Fig. 7(c), significant difference of the T/N ratio between the probe and blocking group was achieved at 48-h (20% blockage effect, $p = 0.023$) PI. Because of the signal interference caused by systemic probe uptake at these time points [Fig. 7(a)], these percentages may not represent the true blocking effect. As such, we will use the *ex vivo* imaging results to evaluate the specificity of ZW760-mbc94 in the living system.

After the last imaging time point (72-h PI), the mice were sacrificed, and the major organs (blood, heart, lung, liver, spleen, pancreas, kidney, muscle from left leg, and brain) were harvested for *ex vivo* biodistribution analysis [Fig. 8(a)]. The fluorescent intensities in tumor and organs were measured, and the signal contrast (fluorescence signal from tumor or organ/signal from muscle) values are presented in Fig. 8(b). Mice treated with ZW760-mbc94 showed an *ex vivo* T/N ratio of 2.88 (2.88 ± 1.20), whereas blocked mice showed a T/N ratio of 1.54 (1.54 ± 0.44), with 47% blocking effect. The free dye control mice showed a T/N ratio of 1.28 (1.28 ± 0.09).

High-signal contrast in the liver was observed in both probe group ($\text{liver}/N = 24.54 \pm 5.56$) and blocking group ($\text{liver}/N = 24.76 \pm 1.44$), whereas the signal contrast in the kidney was much lower ($\text{kidney}/N = 2.69 \pm 0.14$ in the probe group; $\text{kidney}/N = 2.68 \pm 0.29$ in the blocking group). These results indicate that ZW760-mbc94 was cleared mainly from liver. The high-organ uptake caused relatively low *in vivo* tumor imaging contrast [Fig. 7(a)], as compared with the *in vivo* imaging results [Fig. 7(d) and Ref. 26] using our previously reported probe, NIR760-mbc94. Importantly, despite the high-probe uptake in the liver and kidney, blocking effect was only observed in the tumor, indicating specificity of ZW760-mbc94 in the living system.

4 Summary

In summary, we developed a CB_2R-targeted zwitterionic NIR fluorescent probe, ZW760-mbc94, which showed specific binding to the target receptor *in vitro* and *in vivo*. When compared with the charged NIR probe (NIR760-mbc94) that possesses the same targeting moiety, ZW760-mbc94 showed enhanced blocking effect *in vitro* (from 40% to 50%) and *ex vivo* (from 35% to 47%). Overall, ZW760-mbc94 appears to be a promising CB_2R-targeted imaging probe. Moreover, replacing a charged NIR dye

with a zwitterionic one appears to be an effective approach to reduce nonspecific binding.

Acknowledgments

We thank Dr. Nephi Stella at the University of Washington for providing DBT cells and technical advice. We also thank Dr. Xiangqun Xie at the University of Pittsburgh for providing support to this project. This work was supported by the startup fund provided by the Department of Radiology, University of Pittsburgh. This project used the UPCI imaging facilities supported, in part, by award P30CA047904.

References

1. F. Rodriguez de Fonseca et al., "The endocannabinoid system: physiology and pharmacology," *Alcohol Alcohol.* **40**(1), 2–14 (2004).
2. E. L. Scotter, M. E. Abood, and M. Glass, "The endocannabinoid system as a target for the treatment of neurodegenerative disease," *Br. J. Pharmacol.* **160**(3), 480–498 (2010).
3. M. Sexton et al., "NIR-mbc94, a fluorescent ligand that binds to endogenous CB(2) receptors and is amenable to high-throughput screening," *Chem. Biol.* **18**(5), 563–568 (2011).
4. G. Velasco et al., "Cannabinoids and gliomas," *Mol. Neurobiol.* **36**(1), 60–67 (2007).
5. P. Pacher, S. Batkai, and G. Kunos, "The endocannabinoid system as an emerging target of pharmacotherapy," *Pharmacol. Rev.* **58**(3), 389–462 (2006).
6. B. G. Ramirez et al., "Prevention of Alzheimer's disease pathology by cannabinoids: neuroprotection mediated by blockade of microglial activation," *J. Neurosci.* **25**(8), 1904–1913 (2005).
7. T. Sugiura et al., "Evidence for the involvement of the cannabinoid CB_2 receptor and its endogenous ligand 2-arachidonoylglycerol in 12-O-tetradecanoylphorbol-13-acetate-induced acute inflammation in mouse ear," *J. Biol. Chem.* **280**(18), 18488–18497 (2005).
8. H. Iwamura et al., "In vitro and in vivo pharmacological characterization of JTE907, a novel selective ligand for cannabinoid CB_2 receptor," *J. Pharmacol. Exp. Ther.* **296**(2), 420–425 (2001).
9. M. M. Ibrahim et al., "Activation of CB_2 cannabinoid receptors by AM1241 inhibits experimental neuropathic pain: pain inhibition by receptors not present in the CNS," *Proc. Natl. Acad. Sci. U. S. A.* **100**(18), 10529–10533 (2003).
10. M. Karsak et al., "The cannabinoid CB_2 receptor: a potential target for the diagnosis and treatment of osteoporosis," *J. Bone Miner. Res.* **19** (S1), S383–S383 (2004).
11. A. Ortega-Alvaro et al., "Deletion of CB_2 cannabinoid receptor induces schizophrenia-related behaviors in mice," *Neuropsychopharmacology* **36**(7), 1489–1504 (2011).
12. M. S. Garcia-Gutierrez and J. Manzanares, "Overexpression of CB_2 cannabinoid receptors decreased vulnerability to anxiety and impaired anxiolytic action of alprazolam in mice," *J. Psychopharmacol.* **25**(1), 111–120 (2011).
13. M. S. Garcia-Gutierrez et al., "Chronic blockade of cannabinoid CB_2 receptors induces anxiolytic-like actions associated with alterations in GABA(A) receptors," *Br. J. Pharmacol.* **165**(4), 951–964 (2012).
14. Z. X. Xi et al., "Brain cannabinoid CB_2 receptors modulate cocaine's actions in mice," *Nat. Neurosci.* **14**(9), 1160–1166 (2011).
15. B. K. Atwood and K. Mackie, "CB_2: a cannabinoid receptor with an identity crisis," *Br. J. Pharmacol.* **160**(3), 467–479 (2010).
16. D. A. Mankoff, "A definition of molecular imaging," *J. Nucl. Med.* **48** (6), 18N–21N (2007).
17. S. Galiegue et al., "Expression of central and peripheral cannabinoid receptors in human immune tissues and leukocyte subpopulations," *Eur. J. Biochem.* **232**(1), 54–61 (1995).
18. M. F. Bai et al., "MBC94, a conjugable ligand for cannabinoid CB_2 receptor imaging," *Bioconjugate Chem.* **19**(5), 988–992 (2008).
19. J. Guindon and A. G. Hohmann, "The endocannabinoid system and cancer: therapeutic implication," *Br. J. Pharmacol.* **163**(7), 1447–1463 (2011).
20. T. Iuvone et al., "Selective CB_2 up-regulation in women affected by endometrial inflammation," *J. Cell Mol. Med.* **12**(2), 661–670 (2008).
21. S. Steffens et al., "Low dose oral cannabinoid therapy reduces progression of atherosclerosis in mice," *Nature* **434**(7034), 782–786 (2005).
22. A. Ellert-Miklaszewska et al., "Distinctive pattern of cannabinoid receptor type II (CB_2) expression in adult and pediatric brain tumors," *Brain Res.* **1137**(1), 161–169 (2007).
23. M. D. Van Sickle et al., "Identification and functional characterization of brainstem cannabinoid CB_2 receptors," *Science* **310**(5746), 329–332 (2005).
24. C. Benito et al., "Cannabinoid CB_2 receptors and fatty acid amide hydrolase are selectively overexpressed in neuritic plaque-associated glia in Alzheimer's disease brains," *J. Neurosci.* **23**(35), 11136–11141 (2003).
25. C. Benito et al., "Cannabinoid CB_1 and CB_2 receptors and fatty acid amide hydrolase are specific markers of plaque cell subtypes in human multiple sclerosis," *J. Neurosci.* **27**(9), 2396–2402 (2007).
26. S. Zhang, P. Shao, and M. Bai, "In vivo type 2 cannabinoid receptor-targeted tumor optical imaging using a near infrared fluorescent probe," *Bioconjugate Chem.* **24**(11), 1907–1916 (2013).
27. H. S. Choi et al., "Targeted zwitterionic near-infrared fluorophores for improved optical imaging," *Nat. Biotechnol.* **31**(2), 148–153 (2013).
28. H. S. Choi et al., "Synthesis and in vivo fate of zwitterionic near-infrared fluorophores," *Angew. Chem. Int. Edit.* **50**(28), 6258–6263 (2011).
29. E. Cudaback et al., "The expression level of CB_1 and CB_2 receptors determines their efficacy at inducing apoptosis in astrocytomas," *Plos One* **5**(1), e8702 (2010).
30. H. Lee, J. C. Mason, and S. Achilefu, "Heptamethine cyanine dyes with a robust C-C bond at the central position of the chromophore," *J. Org. Chem.* **71**(20), 7862–7865 (2006).
31. M. Ogawa et al., "H-type dimer formation of fluorophores: a mechanism for activatable, in vivo optical molecular imaging," *ACS Chem. Biol.* **4**(7), 535–546 (2009).
32. P. Juzenas et al., "Spectroscopic evidence of monomeric aluminium phthalocyanine tetrasulphonate in aqueous solutions," *J. Photoch. Photobiol. B* **75**(1–2), 107–110 (2004).
33. J. T. Castaneda et al., "Differential expression of intracellular and extracellular CB(2) cannabinoid receptor protein by human peripheral blood leukocytes," *J. Neuroimmune Pharmacol.* **8**(1), 323–332 (2013).

Zhiyuan Wu received his MD degree from Shanghai Jiao Tong University School of Medicine in China and is currently working as a postdoctoral fellow in Dr. Mingfeng Bai's lab at the University of Pittsburgh. His research interests include molecular imaging of cancer and imaging biomarkers research. He has published more than 40 peer-reviewed journal articles in these fields.

Pin Shao is currently a research associate in Dr. Mingfeng Bai's lab at the Department of Radiology, University of Pittsburgh. She obtained her PhD degree in chemistry from Wuhan University, PR China, and her research interests are in the development of novel near-infrared fluorescent compounds for optical and/or photoacoustic imaging, as well as drug delivery.

Shaojuan Zhang earned her PhD degree at Gunma University in Japan and is currently a postdoctoral fellow at University of Pittsburgh, under the mentorship of Dr. Mingfeng Bai. Her research interests are targeted optical imaging and cancer therapeutics using molecular probes.

Mingfeng Bai is an assistant professor of radiology at the University of Pittsburgh. He received his MSc and PhD degrees in chemistry from Vanderbilt University and BS degree in chemistry from Nankai University, PR China. His research group is focused on developing novel molecular imaging probes for diagnostic imaging and phototherapy. He has been successful publishing peer-reviewed journal articles, holds various patents, and has given many presentations nationally and internationally.